Copyright © 2010 Tech Science Press SDHM, vol.6, no.4, pp.239-271, 2010

Efficient Fracture Analysis of 2D Crack Problems by the MVCCI Method

H. Theilig[1]

Abstract: The aim of this paper is to give an overview to some problems and solutions of the fracture analysis of 2D structures. It will be shown that the common computer-aided two-dimensional fatigue crack path simulation can be considerably improved in accuracy by using a predictor-corrector procedure in combination with the *modified virtual crack closure integral* (MVCCI) method. Furthermore the paper presents an improved finite element technique for the calculation of stress intensity factors of mixed mode problems by the MVCCI Method. The procedure is devised to compute the separated strain energy release rates by using the convergence of two separate calculations with different element sizes in the neighborhood of the crack tip. In order to evaluate the validity and efficiency of the proposed higher order crack path simulation method, experiments of curved fatigue crack growth are carried out with a specially designed specimen under proportional lateral force bending. In all cases considered, the computationally predicted crack trajectories show an excellent agreement with the curved cracks that are obtained in the experiments. Additionally the procedure has been extended to analyse the crack growth and the plastic limit load for each crack propagation step in a fully automatic simulation. The proposed solution algorithm provides a powerful tool for flaw assessment with the FAD procedure in combination with a numerical crack path simulation. Several numerical examples are presented to show the accuracy and the efficiency of the crack path simulation including the analysis of the plastic limit loads.

Keywords: Curved cracks, numerical crack path simulation, parabolic increment, predictor-corrector procedure, improved modified virtual crack closure integral method, multiple mesh analysis, plastic limit load, failure assessment diagram

[1] Ingenieurbüro für Angewandte Mechanik, Zittau, Germany

1 Introduction

From failed structures and components it is known in engineering practice that cracks frequently originate and extend in regions characterized by complicated geometrical shapes and asymmetrical loading conditions. Further it is possible, that material flaws or pre-existing cracks which may have been formed during the manufacturing process often have initial mixed mode loading conditions under operating exposure. In such cases, the developing crack paths are found to be curved and the well known standard solutions for straight cracks [Theilig and Nickel (1987)] do not apply.

The 3rd edition of the German FKM-Guideline "Fracture Mechanics Proof of Strength for Engineering Components" includes several recommendations for the treatment of pre-existing cracks with mixed mode loading and for the use of the well known 2-parameter- approach of the failure assessment diagram in such case, [Berger, Blauel, Hodulak, Pyttel and Varfolomeyev (2006)]. Further notes are given for the analysis of crack growth as the consequence of cycling loading by numerical simulation. It is well known, that a complete description of the expected fracture behaviour of cracked components can be solved only by coupling of crack growth with rules for the evolution of the crack geometry. The concepts for the simulation of the geometrical evolution of cracks usually are based on the criterion of local symmetry [Goldstein and Salganik (1974)]. In addition to these fracture mechanical criterion geometrical constraints must be considered on continuous crack growth, which are discussed extensively by Hull (1993).

Several numerical methods like the finite element method, the extended finite element method, the boundary element method or meshless methods were successfully applied for the step-by-step simulation of curved crack propagation [Bergkvist and Gnex (1978), Sumi (1985), Schöllmann, Fulland and Richard (2003), Colombo and Giglio (2006), Moës, Dolbow and Belytschko (1999), Aliabadi (2002), Rao and Rahman (2000)]. Especially a predictor–corrector procedure based on finite elements was proven to be very accurate and robust in computing single cracks and multiple crack systems [Theilig, Döring and Buchholz (1997), Theilig, Wünsche and Bergmann (2003), Theilig and Wünsche (2003)]. The method uses a higher order simulation concept with curved increments and was implemented in the code PCCS-2D.

The results of crack path simulations are usually only the histories of stress intensity factors K_I as a function of the changing crack geometry and the given loading system. Evaluations with the FAD, however, will be possible only with a complementary numerical analysis of plastic limit loads. In order to solve such problems in cases with curved interacting cracks, the crack path simulation code PCCS-2D

has been extended to an additional analysis of the plastic limit load at every step of the numerical simulation [Theilig, Holländer and Wünsche (2010)].

2 Two-dimensional crack path simulation

2.1 2D crack problem

Consider a system of M interacting crack tips in a two-dimensional linear elastic component under initial mixed mode condition. The stresses ahead of the lth crack tip are given by

$$\sigma_{11}(x_1^l,0) = \frac{k_I^l}{\sqrt{2\pi x_1^l}} + T^l + b_I^l \sqrt{\frac{x_1^l}{2\pi}} + O(x_1^l),$$

$$\sigma_{22}\left(x_1^l,0\right) = \frac{k_I^l}{\sqrt{2\pi x_1^l}} + b_I^l \sqrt{\frac{x_1^l}{2\pi}} + O\left(x_1^l\right), \tag{1}$$

$$\sigma_{12}\left(x_1^l,0\right) = \frac{k_{II}^l}{\sqrt{2\pi x_1^l}} + b_{II}^l \sqrt{\frac{x_1^l}{2\pi}} + O\left(x_1^l\right)$$

where k_I^l and k_{II}^l are the *stress intensity factors* (SIFs). T^l, b_I^l and b_{II}^l are the included higher order stress field parameters. It is known that in such a situation the cracks will propagate in a smoothly curved manner after an abrupt deflection out of its original planes, Fig. 1.

2.2 Initial crack kinking

From the literature several hypotheses are well known for the prediction of the crack kinking under mixed-mode loading conditions. The most widely used of these are:

a) the maximum tangential stress criterion,

b) the strain energy density criterion,

c) the maximum energy release rate criterion and

d) the local symmetry criterion.

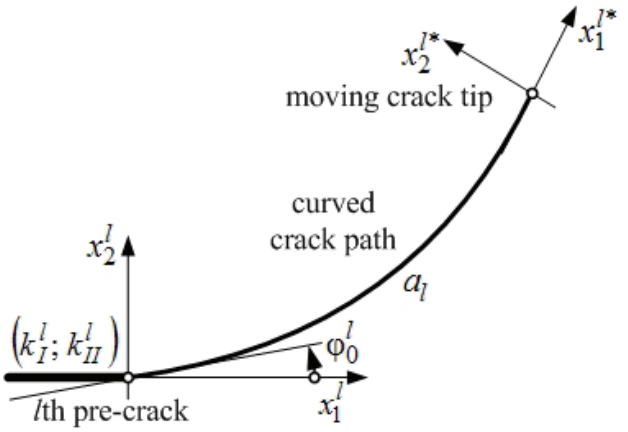

Figure 1: A kinked and curved crack

In addition to the instability criterion, each hypotheses formulate a statement about the initial direction φ_0 of crack propagation. These criteria are of two principally different types.The first category evaluates the stress field around the original crack tip and determinates the direction by means of the local distribution of characteristic field parameters. The propagation direction is found for instance from the position of the maximum tangential stress (a) or the minimum strain energy density (b). The second category is due to virtual infinitesimal small kinked crack extension. That direction of the straight kinked crack extensions is regarded as real at which the elastic strain energy release rate reaches a maximum (c) or the stress intensity factor of the in-plane shear mode vanishes (d).

For several mixed-mode fracture criteria the initial direction φ_0^l depends only on the ratio k_{II}^l/k_I^l of the SIFs of the original crack, whereas for others a further dependence on Poisson's ratio ν is found. Well known is the maximum tangential stress criterion, [Erdogan and Sih (1963)], with

$$\varphi_0^l = -\arccos\left(\frac{3k_I^{l\,2} + k_I^l\sqrt{k_I^{l2} + 8k_{II}^{I\,2}}}{k_I^{l2} + 9k_{II}^{l\,2}}\right) \tag{2}$$

and

$$K_I^l = K_{eq}^l = \cos\frac{\varphi_0^l}{2}\left(k_I^l\cos^2\frac{\varphi_0^l}{2} - \frac{3}{2}k_{II}^l\sin^2\varphi_0^l\right) \tag{3}$$

as the equvivalent mode I stress intensity factor. For small ratios $0<|k_{II}^l/k_I^l|<0.1$ practically the same values $\varphi_0^l = -2k_{II}^l/k_I^l$ are predicted by all criteria [Bergkvist

and Gnex (1978)]. This means, that under these conditions all criteria results in the state of local symmetry at the branched actual crack tip.

2.3 Curved mode I crack growth

For the curved evolution of crack paths in a homogeneous isotropic material under monotonic or cyclic proportional loading the generalisation of the local symmetry criterion can be regarded as the natural basis. Thus, it can be stated that a continuously growing crack will form a path that experiences pure mode I at any crack tip position, Fig. 1. Therefore, the states of stress ahead of the deflected new crack tips exhibit no inplane shear mode and are given by

$$\sigma_{11}(x_1^{l*},0) = \frac{K_I^l}{\sqrt{2\pi x_1^{l*}}} + T^{l*} + b_I^{l*}\sqrt{\frac{x_1^{l*}}{2\pi}} + O(x_1^{l*}),$$

$$\sigma_{22}\left(x_1^{l*},0\right) = \frac{K_I^l}{\sqrt{2\pi x_1^{l*}}} + b_I^{l*}\sqrt{\frac{x_1^{l*}}{2\pi}} + O\left(x_1^{l*}\right), \tag{4}$$

$$\sigma_{12}\left(x_1^{l*},0\right) = b_{II}^{l*}\sqrt{\frac{x_1^{l*}}{2\pi}} + O\left(x_1^{l*}\right).$$

The Cartesian crack front coordinate system (x_1^{l*}, x_2^{l*}) is defined with the origin at the actual lth crack tip with the x_1^{l*}-axis along the tangential direction of the crack path. It can be stated that continuous crack deflection can be caused only by the existing non-singular stresses.

According to [Sumi and Wang (1998)], the prediction of cracking formation of a system of interacting cracks can be performed by using a first order perturbation solution of slightly kinked and curved extensions of all growing cracks, which analytical gives the virtual mixed mode stress intensity factors $\bar{K}_I^l$ and $\bar{K}_{II}^l$ at all arbitrarily extended crack tips.

A virtual extended slightly kinked and smoothly curved crack path profile is assumed in the form

$$\lambda_l\left(x_1^l\right) = \alpha^l x_1^l + \beta^l \left(x_1^l\right)^{3/2} + \gamma^l \left(x_1^l\right)^2 + O\left(\left(x_1^l\right)^{5/2}\right) \tag{5}$$

at the lth crack tip, where α^l, β^l and γ^l are the chosen shape parameters, Fig. 2. The projected crack length on the x_1^l-axis is represented by h_l.

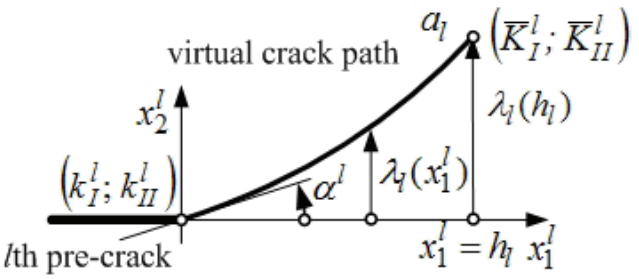

Figure 2: Virtual extended lth crack

With $\bar{K}_{II}^l(x_1^l) = 0$ and $0 \le x_1^l \le h_l$ for each extended crack tip ($l = 1,\ldots,M$) the shape parameters of the natural crack paths are obtained as

$$\alpha^l = -2\,k_{II}^l/k_I^l, \tag{6}$$

$$\beta^l = \frac{8}{3}\sqrt{\frac{2}{\pi}}\,\frac{T^l}{k_I^l}\,\alpha^l, \tag{7}$$

$$\gamma^l = \frac{1}{k_I^l}\left\{\frac{3\sqrt{2\pi}}{4}\beta_l T^l - \frac{1}{2}b_{II}^l + \frac{1}{4}\alpha^l b_I^l\right.$$

$$-\sum_{m=1}^{M}\left[(k_I^m - \alpha^m k_{II}^m)\bar{k}_{21}^{lm} + (k_{II}^m - \alpha^m k_I^m)\bar{k}_{22}^{lm} + \frac{1}{2}\alpha^m k_I^m \bar{k}_{11}^{lm}\right.$$

$$\left.\left.+\frac{1}{2}\alpha^m k_{II}^m \bar{k}_{12}^{lm}\right]\frac{h_m}{h_l}\right\}. \tag{8}$$

It is seen that α^l is equivalent to the initial direction $\varphi_0^l = -2k_{II}^l/k_I^l$ for small ratios $|k_{II}^l/k_I^l|$. Based on a numerical analysis of the stress field parameters $k_I^l, k_{II}^l, T^l, b_I^l, b_{II}^l$ and $\bar{k}_{ij}^{lm}$ with i, j = 1,2 and l, m = 1,..., M at the initial crack tips Sumi and Wang (1998) formulate a step by step simulation procedure with piecewise curvilinear shape.

The simulation can be simplified considerably by the analysis of the curved pure mode I crack growth [Theilig, Döring, and Buchholz (1997)]. If we consider initial cracks under local symmetry, i.e. $k_{II}^l = 0$, we find $\alpha_I^l = 0,\ \beta_I^l = 0$, Fig. 3.

Therefore the parabolic crack profiles

$$\lambda_l(x_1^l) = \gamma^l\,(x_1^l)^2 \tag{9}$$

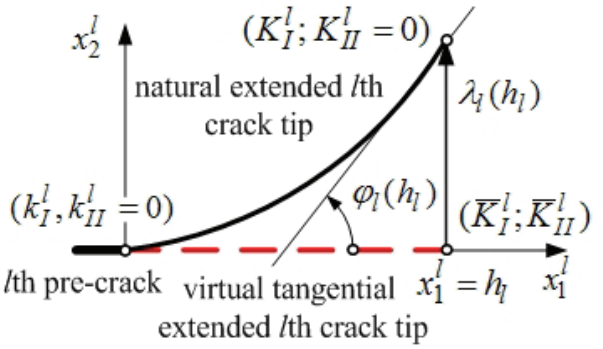

Figure 3: Curved crack growth under local symmetry at the initial crack tips

are obtained, with

$$\gamma^l = -\frac{1}{k_I^l}\left(\frac{1}{2}b_{II}^l + \sum_{m=1}^{M} k_I^m \bar{k}_{21}^{lm}\,\frac{h_m}{h_l}\right) \tag{10}$$

and

$$K_I^l = k_I^l + \frac{1}{2}b_I^l h_l + \sum_{m=1}^{M} k_I^m \bar{k}_{11}^{lm} h_m, \tag{11}$$

This means, that all interacting cracks will propagate with continuous natural deflections without mixed mode loading. Further it is seen, that the curvature of each crack is affected by the other growing cracks. Therefore the relative crack propagation rate h_m/h_l must be evaluated under the condition of natural simultaneous growth of all moving cracks.

Further in the case of tangential virtual crack extensions h_l the virtual SIFs

$$\bar{K}_I^l = k_I^l + \frac{1}{2}b_I^l h_l + \sum_{m=1}^{M} k_I^m \bar{k}_{11}^{lm} h_m, \tag{12}$$

$$\bar{K}_{II}^l = \frac{1}{2}b_{II}^l h_l + \sum_{m=1}^{M} k_I^m \bar{k}_{21}^{lm} h_m \tag{13}$$

are obtained. From equations (11) and (12) $K_I^l(h_l) = \bar{K}_I^l(h_l)$ is found as the consequence of the considered slightly curved crack extensions. Further follows with known $\bar{K}_{II}^l(h_l)$ from (10) and (13)

$$\gamma^l = -\frac{\bar{K}_{II}^l}{k_I^l h_l}. \tag{14}$$

One gets finally according to Fig. 3 the geometrical quantities of the crack trajectories at the crack tip:

$$\varphi_l(\mathrm{h_l}) = -2\,\frac{\bar{K}_{II}^l}{k_I^l}, \tag{15}$$

$$\lambda_l(h_l) = -\frac{\bar{K}_{II}^l}{k_I^l} h_l, \tag{16}$$

$$a_l(h_l) \approx h_l \left[1 + \frac{2}{3}\left(\frac{\bar{K}_{II}^l}{k_I^l}\right)^2 - \frac{2}{5}\left(\frac{\bar{K}_{II}^l}{k_I^l}\right)^4\right]. \tag{17}$$

2.4 Curved crack path simulation

Based on the equations (15), (16) and (17) the simulation of the curved crack growth of interacting cracks can be carried out by a *predictor-corrector method* (PCM) [Theilig and Wünsche (2005)]. The predictor-step is the realization of a compatible set of small simultaneous virtual tangential crack extensions. The corrector-step follows with the calculation of the resulting crack paths and with the preparation of the next virtual crack extensions. In conjunction with the related tangential crack extensions $\Delta h_{l,j}$ only the numerical calculation of $K_{Ij}^l = \bar{K}_{Ij}^l$ and $\Delta\bar{K}_{IIj}^l$ is necessary.

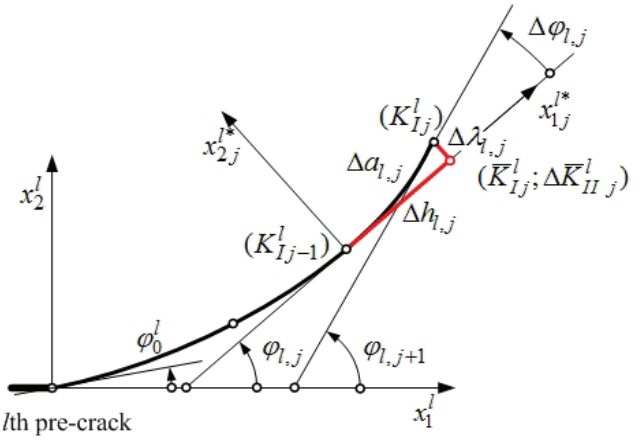

Figure 4: Step by step approach with curved increment

According to Fig. 4, the following equations of the step-by-step strategy can be derived:

$$\varphi_{l,j+1} = \varphi_{l,j} - 2\frac{\Delta\bar{K}^l_{II_j}}{K^l_{I\,j-1}}, \tag{18}$$

$$\lambda_{l,j} = -\frac{\Delta\bar{K}^l_{II\,j}}{K^l_{I\,j-1}}\,\Delta h_{l,j}, \tag{19}$$

$$a_{l,j} = a_{l,j-1} + \left[1 + \frac{2}{3}\left(\frac{\Delta\bar{K}^l_{II\,j}}{K^l_{I\,j-1}}\right)^2 - \frac{2}{5}\left(\frac{\Delta\bar{K}^l_{II\,j}}{K^l_{I\,j-1}}\right)^4\right]\Delta h_j. \tag{20}$$

with j as the simulation step number. It should be noted that K^l_{I0} results from the equivalent stress intensity factors K^l_{Ieq} of the pre-existing mixed mode loaded cracks after (3). The crack path simulation strategy with straight incremental steps follows without the proposed correction:

$$\varphi_{l,j+1} = \varphi_{l,j} - 2\frac{\Delta\bar{K}^l_{II\,j}}{K^l_{I\,j-1}}, \tag{21}$$

$$a_{l,j} = a_{l,j-1} + \Delta h_{l,j}. \tag{22}$$

It can be seen that equation (21) is different to those of the well known common method based on a repeated *mixed mode interpretation* (MMI):

$$\varphi_{l,j+1} = \varphi_{l,j} - 2\frac{K^l_{II\,j}}{K^l_{I\,j}}\ , \tag{23}$$

$$a_{l,j} = a_{l,j-1} + \Delta h_{l,j}. \tag{24}$$

The maximum amount of virtual crack extension increment Δh_{lmax} should be taken for the crack tip l_{max}, where the maximum stress intensity factor $K_I^{l\max}$ occurs.

Using the Paris law with a user-defined number of loading cycles ΔNwe obtain for the step j

$$\Delta h_{l\max,j} = C\left[K^{l\max}_{Ij}(1-R)\right]^n \Delta N,\ \ R = \frac{\sigma_{\min}}{\sigma_{\max}}, \tag{25}$$

$$\Delta h_{l,j} = \Delta h_{l\max,j}\left(\frac{K^l_{Ij}}{K^{l\max}_{Ij}}\right)^n. \tag{26}$$

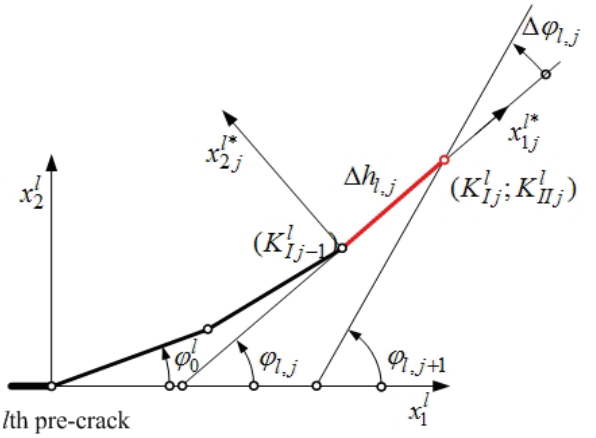

Figure 5: Step by step approach with mixed mode interpretation

2.5 Improved MVCCI method

By considering equations (18), (19) and (20) it can be clearly seen, that the simulation of crack growth requires highly accurate stress intensity factors in order to reduce numerical errors in the computation of the crack extension increments. Further an efficient numerical mode separation technique in conjunction with the step-by-step analysis is necessary. For this reason an improved MVCCI method [Theilig, Wünsche and Bergmann (2003)] was developed, which provides a highly accurate computation of the separated strain energy release rates and the related stress intensity factors without special techniques also in cases of models with course meshing.

For 8-noded quadrilaterals at the crack tip, which are necessary to model the parabolic curved increments of the crack path, the following first and second order finite element representation of Irwin's crack closure integral relations can be given for a crack closure length Δa and the thickness t of the plane model at the crack front, Fig.6:

$$G_I^{(1)}(a) = \frac{1}{2t\Delta a}\left(\mathrm{F}_{2,\mathrm{i}}\Delta\mathrm{u}_{2,\mathrm{i}-2} + \mathrm{F}_{2,\mathrm{i}+1}\Delta\mathrm{u}_{1,\mathrm{i}-1}\right), \tag{27}$$

$$G_{II}^{(1)}(a) = \frac{1}{2t\Delta a}\left(\mathrm{F}_{1,\mathrm{i}}\Delta\mathrm{u}_{1,\mathrm{i}-2} + \mathrm{F}_{1,\mathrm{i}+1}\Delta\mathrm{u}_{1,\mathrm{i}-1}\right), \tag{28}$$

$$G_I^{(2)}(a) = \frac{1}{2t\Delta a}\left(F_{2,i}\Delta u_{2,i-4} + F_{2,i+1}\Delta u_{2,i-3} + F_{2,i+2}\Delta u_{2,i-2} + F_{2,i+3}\Delta u_{2,i-1}\right), \tag{29}$$

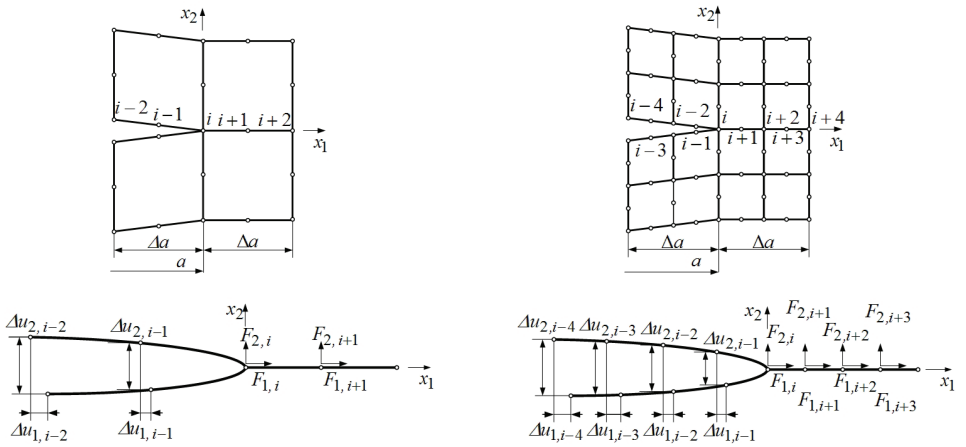

(a) (b)

Figure 6: First (a) and second (b) order evaluation of the MVCCI method

$$G_{II}^{(2)}(a) = \frac{1}{2t\Delta a}\left(F_{1,i}\Delta u_{1,i-4} + F_{1,i+1}\Delta u_{1,i-3} + F_{1,i+2}\Delta u_{1,i-2} + F_{1,i+3}\Delta u_{1,i-1}\right). \quad (30)$$

It is well known that in the case of a plane crack problem the convergence in the strain energy W_f of the finite element solution is of order h_e , where h_e is the size of the elements adjacent to the crack tip, Fig. 7 [Tong and Pian (1973)]. With the displacements of the unknown exact solution $\mathbf{u}_{EX}$ and those of the finite element solution $\mathbf{u}_{FEM}$ we have:

$$W_f(\mathbf{u}_{FEM} - \mathbf{u}_{EX}) \leq ch_e. \quad (31)$$

If we assume a solution by the conventional finite element displacement method it follows that

$$W_f(\mathbf{u}_{FEM} - \mathbf{u}_{EX}) = W_f(\mathbf{u}_{EX}) - W_f(\mathbf{u}_{FEM}). \quad (32)$$

As the result of two separate finite element calculations for a given crack length a with different element subdivisions h_{e1} and h_{e2} in the neighbourhood of the crack tip, one obtains with

$$W_f^{EX}(a) = W_f(\mathbf{u}_{EX}), \quad W_f^{(1)}(a) = W_f(\mathbf{u}_{FEM1}), \quad W_f^{(2)}(a) = W_f(\mathbf{u}_{FEM2})$$

and

$$W_f^{EX}(a) \geq W_f^{IMPR}(a) > W_f^{(2)}(a) > W_f^{(1)}(a)$$

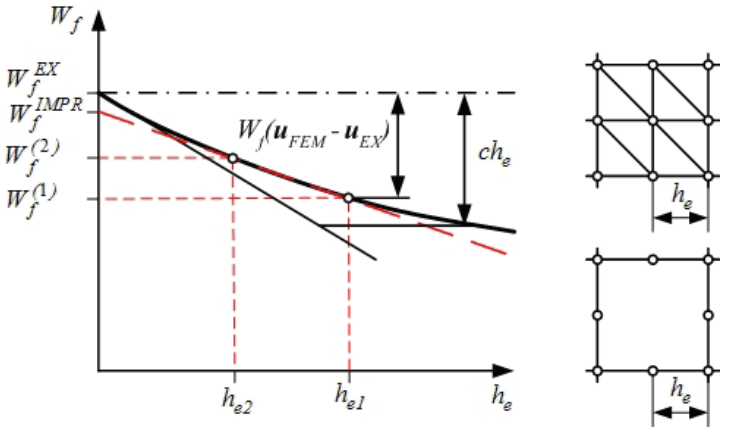

Figure 7: Convergence of the strain energy W_f for a plane crack problem in the case of a solution by the conventional finite element displacement method

the improved approximate strain energy

$$W_f^{IMPR}(a) = \frac{W_f^{(1)}(a) - W_f^{(2)}(a)\frac{h_{e1}}{h_{e2}}}{1 - \frac{h_{e1}}{h_{e2}}} \tag{33}$$

[Theilig (1981, 1982, 1984)]. Therefore it is possible to obtain separated improved strain energy release rates by a first and a second order evaluation of the MVCCI method for the same crack closure length Δa with different element sizes $h_{e1} > h_{e2}$:

$$G_I^{IMPR}(a) = \frac{G_I^{(1)}(a) - G_I^{(2)}(a)\frac{h_{e1}}{h_{e2}}}{1 - \frac{h_{e1}}{h_{e2}}}, \tag{34}$$

$$G_{II}^{IMPR}(a) = \frac{G_{II}^{(1)}(a) - G_{II}^{(2)}(a)\frac{h_{e1}}{h_{e2}}}{1 - \frac{h_{e1}}{h_{e2}}}. \tag{35}$$

Especially with $h_{e1}/h_{e2} = 2$ one obtains the simple formulas

$$G_I^{IMPR}(a) = 2G_I^{(2)}(a) - G_I^{(1)}(a), \tag{36}$$

$$G_{II}^{IMPR}(a) = 2G_{II}^{(2)}(a) - G_{II}^{(1)}(a). \tag{37}$$

The SIFs K_I and K_{II} can then be calculated from the improved strain energy release rates with

$$K_I^{IMPR}(a) = \sqrt{E^* G_I^{IMPR}(a)}, K_{II}^{IMPR}(a) = \sqrt{E^* G_{II}^{IMPR}(a)} \tag{38}$$

with $E^* = E$ for a plane stress FE-model and $E^* = E/(1-\nu^2)$ in the case of a plane strain FE-model. E is the Young's modulus. The essential feature of this technique is the higher accuracy of the SIFs, which can be obtained by comparatively coarse meshes.

2.6 Analysis of the plastic limit load

In a failure assessment diagram (FAD) an assessment point with the parameters $K_r = K/K_{mat}$ and $L_r = \sigma/\sigma_e$ is compared with a failure line, which is calculated from the material tensile properties. K is the stress intensity factor K_I in a mode I case. In cases with initial mixed mode loading the equivalent stress intensity factor K_{eq} should be taken. The tensile stress σ stands for the loading of the component and σ_e is the corresponding global plastic limit load, which has to be calculated for an elastic-perfectly plastic material model with the lower bound theorem of plasticity. Only primary loads are taken into account. For the given 2D crack problems plane stress and von Mises plasticity are considered. The plastic limit load is evaluated numerically from the characteristic non-linear load-deformation curve. As the deformation parameter the CTOD of the crack tip l_{max} with the maximum stress intensity factor $K_I^{l\max}$ is chosen. Based on the calculated elastic slope a plastic slope criterion is used.

2.7 Implementation of the algorithm

The given approach has been implemented in the program PCCS-2D to run within the FE-code ANSYS [Theilig, Döring and Buchholz (1997), Theilig, Wünsche, and Bergmann (2003), Theilig and Wünsche (2005)]. A fully automatic strategy for proportional loading systems requires no user interaction to predict the incremental extends and the further geometries of all growing cracks.

After each predictor step of virtual tangential crack extensions $\Delta h_{l,j}$ local re-meshing is necessary so that the corrector step is realised in order to model the curved crack surfaces and so that together with the following predictor step new crack tip elements are generated providing additional nodes, Fig. 8. In the case of a second order evaluation of the MVCCI method it is necessary only to halve the given finite element mesh with the crack closure lengths $\Delta h_{l,j}$ at the neighbourhood of the crack tips.

Based on the given modular concept of PCCS-2D a simple iterative solution strategy for proportional loading systems has been developed complementary to analyse the plastic limit load at every simulation step [Theilig, Holländer and Wünsche (2010)].

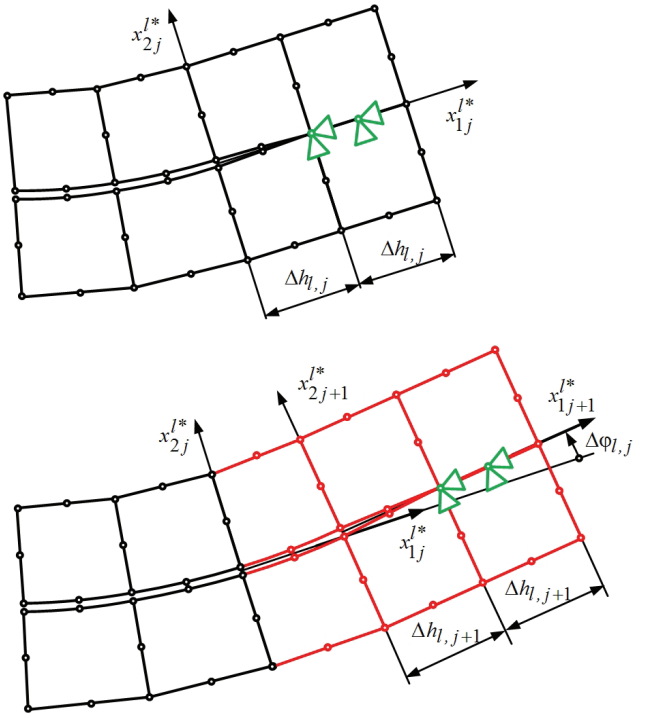

Figure 8: Meshing strategy of the predictor-corrector method

3 Experimental and numerical verification

3.1 Improved calculation of stress-intensity factors

To verify the proposed improved MVCCI method at first a study of the convergence rate in strain energy of a centre cracked rectangular sheet under pure tension will be given in Fig. 9a. Due to double symmetry only a quarter of the sheet was analysed. The numerical results are given in Fig. 9b. The convergence rates in the strain energy are linear functions of h_e as given in equation (31).

As an example some results are given for a rectangular sheet which contains a slant crack, Fig. 10 and Table 1. In this case the proposed procedure is about 100 times

more efficient in terms of relative CPU time used in solving a refined mesh to give results of comparable accuracy.

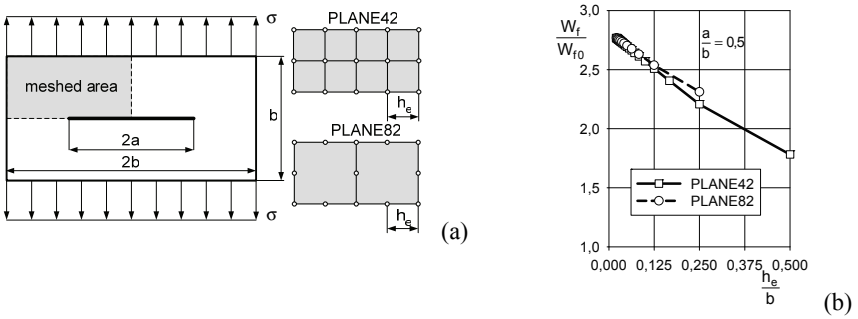

Figure 9: Convergence of the normalised strain energy W_f/W_{f0} of a centre cracked rectangular sheet under uniform uniaxial tensile stress in the case of a solution by the displacement method

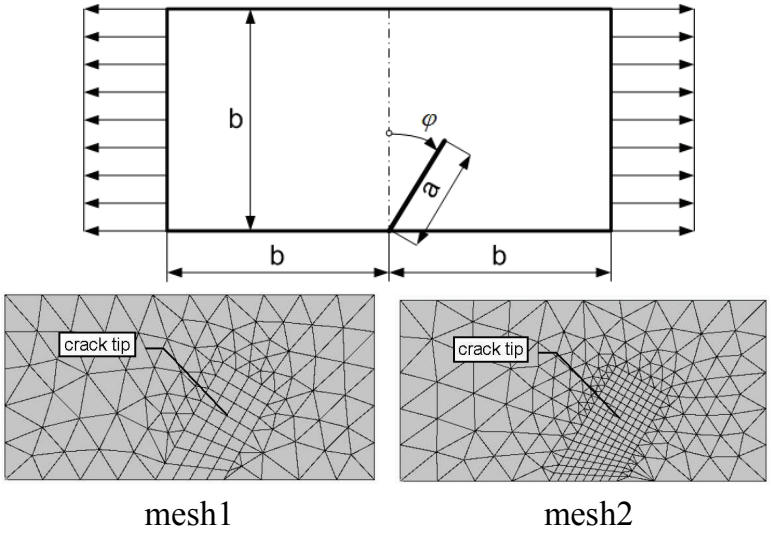

Figure 10: Rectangular sheet with an edge slant crack under uniform tensile stress with finite element meshes mesh1 and mesh2 (PLANE 82), $a = b/2$, φ = 30°, $h_{e1} = a/10$, h_{e1}/h_{e2} =2

Table 1: Accuracy of the normalised stress intensity factors f_I and f_{II} by the MVCCI method for the rectangular sheet with an edge slant crack under uniform tensile stress, $K_I = \sigma_0\sqrt{\pi a} f_I$, $K_{II} = \sigma_0\sqrt{\pi a} f_{II}$, f_I = 1.54, $f_{II} = 0.4$

	$\Delta a/a$	f_I	f_{II}	CPU time/%
First order MVCCI (N1)	0.010	1.533	0.470	100.0
	0.025	1.523	0.469	7.7
	0.050	1.525	0.467	2.7
	0.100	1.515	0.464	1.0
	0.150	1.505	0.460	0.9
	0.200	1.495	0.455	0.8
Second order MVCCI (N2)	0.010	-	-	-
	0.025	1.533	0.470	37.9
	0.050	1.530	0.469	8.3
	0.100	1.525	0.467	2.4
	0.150	1.520	0.464	1.6
	0.200	1.516	0.462	1.1
Improved MVCCI (N1,N2)	0.010	-	-	-
	0.025	1.535	0.471	47.8
	0.050	1.535	0.471	11.0
	0.100	1.535	0.471	2.9
	0.150	1.535	0.470	2.0
	0.200	1.536	0.469	1.6

3.2 Crack path simulation

In order to evaluate the validity and the efficiency of the proposed higher-order crack path simulation method with respect to the well-established basic strategies, experiments of non-coplanar fatigue crack growth were carried out with a specially designed specimen under proportional cyclic *lateral force bending* (LFB). The design of the specimen contains a *hole* in the centre (LFBH) as seen in Fig. 11. Structural steel E335 was selected as specimen material. Crack initiation from notches at different positions a_N along the tensile loaded edge of these specimens was investigated to produce different crack interactions with the given hole. The notches were manufactured with a width of 0.4 mm and a depth of 6 mm by wire-electro discharge machining.

In Fig. 12, 13 and 14 LFBH specimens are shown with experimentally obtained

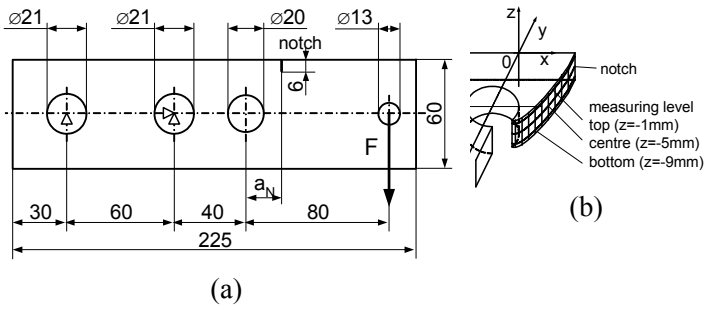

Figure 11: Dimensions and definition of the notch position a_N (a) and the measuring levels (b) of the LFBH specimen (thickness $t = 10$ mm)

curved fatigue crack path for three tested notch positions as examples. It can be recognised that the fatigue cracks are slightly twisted over the thickness of the specimen as the consequence of a disturbance by torsion. But the crack path scattering at the centre line of all specimens tested for each notch position is very small.

For the finite element simulations, the models are chosen in accordance with the design of the specimens and the available test assembly. Fig. 15 shows as an example the finite element meshes of the LFBH specimen with a_N = 30 mm) after 3, 6, 9 and 12 steps of simulated incremental crack growth with Δh = 4mm.

In Fig. 16, 17 and 18 the simulated crack trajectories for the specimens with notch positions a_N = 0, 18 and 30mm are shown together with the experimentally obtained scatter bands from the related fatigue crack growth experiments. For all chosen increments Δh (1mm, 2mm, 4mm) an excellent agreement is found with the proposed predictor-corrector-method. In particular for specimens with notch positions a_N = 30 mm the predictor-corrector method with the first order MVCCI method already results in a very accurate crack path. This is obvious, because in relation to equations (18), (19) und (20) it can be stated out that the numerical errors of the virtual $\Delta\bar{K}_{IIj}$ and the real K_{Ij-1} are about of the same magnitude. Nevertheless it was found that especially as a consequence of the improved MVCCI method with the multiple mesh analysis (h_{e1}/h_{e2} = 2) the computed relation $K_I(a)$ is very accurate also in the case of the step width Δh = 4mm, Tab. 2.

3.3 Global plastic limit load

The used iterative solution strategy for the numerical calculation of the plastic limit load was applied to several cracked components in order to verify its effectiveness. In Tab. 3 the results of the numerical simulation of a centrally cracked strip (Fig. 19)

Table 2: Effect of the calculation method and the step width Δh on the normalised mode I SIF of LFBH specimen a_N = 30mm (crack path simulation by the PCM)

	a/b	$K_I / \sigma_b \sqrt{\pi a}$		
		Δh=1 mm	Δh=2 mm	Δh=4 mm
First order MVCCI	0.0970	0.62526	0.61953	0.61125
	0.1637	0.65671	0.65342	0.64479
	0.2303	0.71541	0.71265	0.70484
	0.2970	0.79879	0.79619	0.78721
	0.3637	0.90671	0.90407	0.89377
	0.4303	1.03973	1.03678	1.02406
	0.4970	1.19753	1.19416	1.17843
	0.5637	1.37932	1.37526	1.35597
	0.6303	1.58657	1.58249	1.56193
	0.6970	1.84804	1.84244	1.82346
	0.7637	2.29515	2.27448	2.23815
	0.8303	3.20800	3.16164	3.05824
	0.8970	5.23211	5.11896	4.86954
Improved MVCCI	0.0970	0.63035	0.63056	0.62988
	0.1637	0.66099	0.66221	0.66211
	0.2303	0.71972	0.72141	0.72261
	0.2970	0.80345	0.80566	0.80593
	0.3637	0.91216	0.91472	0.91565
	0.4303	1.04589	1.04893	1.04856
	0.4970	1.20495	1.20799	1.20678
	0.5637	1.38701	1.39075	1.38813
	0.6303	1.59600	1.59935	1.59934
	0.6970	1.86104	1.86208	1.86566
	0.7637	2.31025	2.30614	2.29446
	0.8303	3.23841	3.22653	3.17993
	0.8970	5.30440	5.27075	5.15710

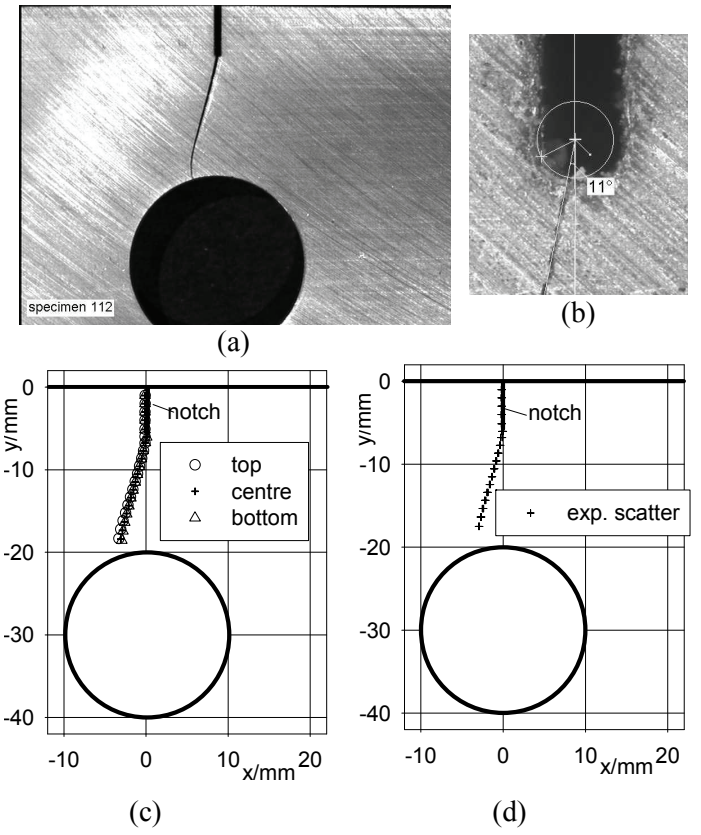

Figure 12: Experimental results of specimen 112, a_N = 0mm, (a) fatigue crack path, (b) initial kinking, (c) measurements, d) experimental scatter (centre line) of all tested specimens.

are given. The simulated crack path is straight as expected. The comparison of the results with those of the FKM guideline shows the achieved quality.

4 Numerical examples

4.1 Stiffened panel

An example of multiple crack propagation in a finite panel with riveted stiffeners has been studied in [Aliabadi (2002)], Fig. 20a. All dimensions in the Figure are given in mm. The sheet and the stiffeners are made of Aluminium alloy A2024-T3. The thickness of the sheet is 2.3mm and the stiffener cross sectional area is 300mm^2. In our case the initial crack lengths are chosen as a_{01}= 12.5mm,

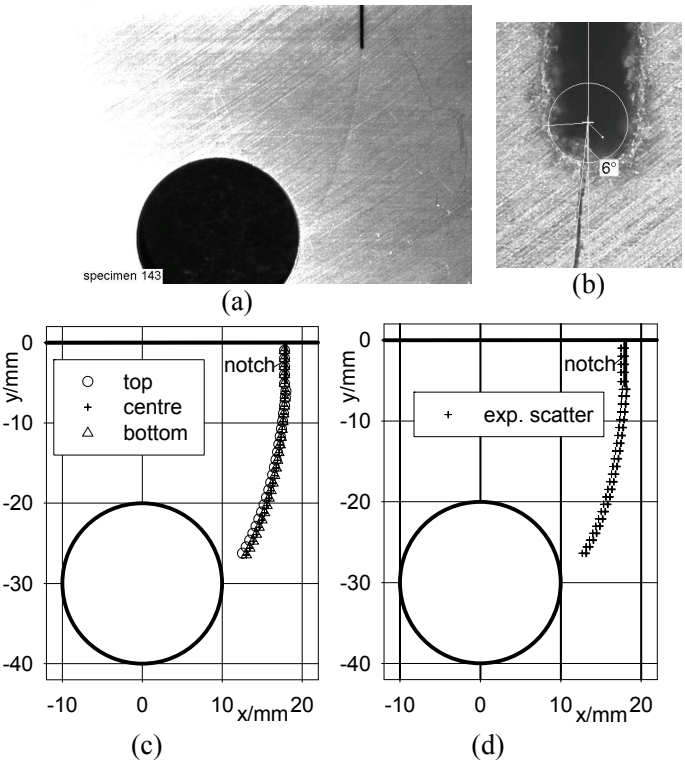

Figure 13: Experimental results of specimen 143, a_N = 0mm, (a) fatigue crack path, (b) initial kinking, (c) measurements, d) experimental scatter (centre line) of all tested specimens.

a_{02}= 12.5mm and a_{03}= 10mm. The panel is subjected to tensile stresses σ_0 of value 10N/mm^2. The stress ratio R is equal to zero. In order to assess the influence of the virtual tangential extension size, the problem was analysed with Δh_{lmax}= 6mm and Δh_{lmax}= 4mm [Theilig and Wünsche (2005)]. In Fig. 20b, c the computationally simulated crack trajectories for the three interacting cracks are shown. The non-dimensional stress intensity factor of crack3 is given Fig. 21, were $f_{I3}= K_{I3}/\sigma_0(\pi a_{3eq})^{1/2}$. The equivalent crack lengths a_{3eq} is the projected length of the curved crack3 on the x-axis. A very good agreement is given with the results of the DBEM in [Aliabadi (2002)].

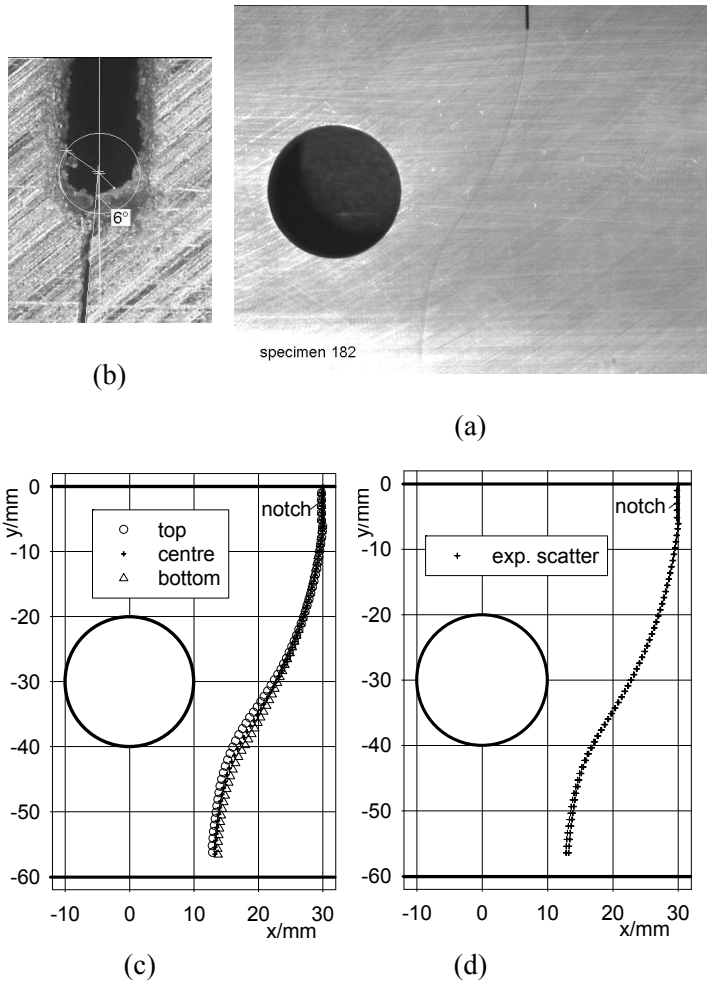

Figure 14: Experimental results of specimen 182, a_N = 0mm, (a) fatigue crack path, (b) initial kinking, (c) measurements, d) experimental scatter (centre line) of all tested specimens.

4.2 Cracks emanating from loaded fastener holes

Especially curved cracks emanating from loaded fastener holes in sheets are analysed in [Theilig, Goth and Wünsche (2006)]. Uniform far field plane stress loading on the sheet and different pin loading on the fastener holes periphery are to be applied. Short cracks (a_0=0.5mm) are assumed as initial mixed mode cracks and fatigue crack growth was simulated until long curved interacting cracks are formed

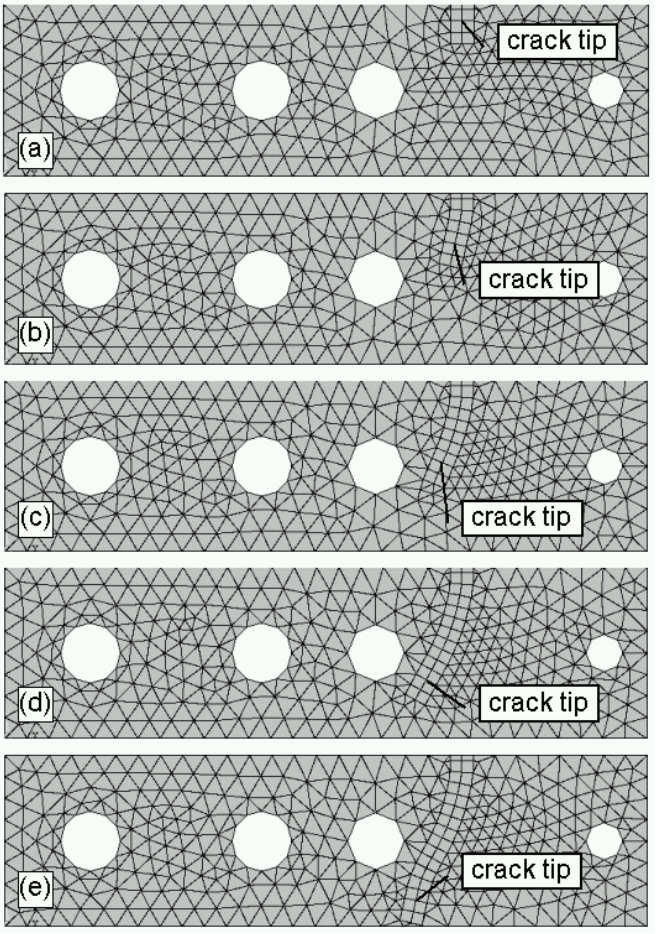

Figure 15: Meshing of the LFBH specimen a_N = 30mm with simulated extension steps Δh = 4mm (first order MVCCI method), (a) initial crack (notch), (b) predictor step 3, (c) predictor step 6, (d) predictor step 9, (e) predictor step 12

near the fastener holes.

At first the contact problem between a fastener and a hole with a single initial crack has been studied, Fig. 22. In nature the loading is highly conformal with a large arc of contact and models with concentrated forces cannot be used. Therefore a model with a given pressure function $p(\phi)$ has been analysed. The normalised mode I stress intensity factor and the simulated crack path are given in Fig. 22b and c.

As a further example multiple crack propagation in a finite sheet with three cracked

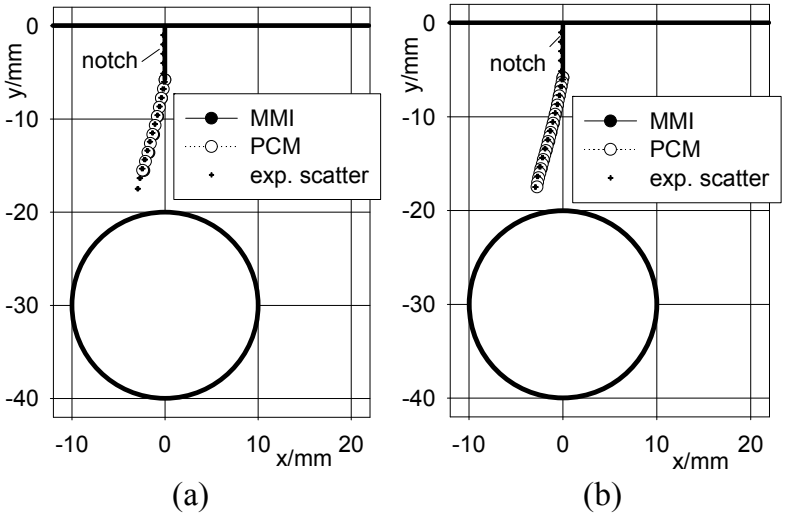

Figure 16: Simulated crack paths of LFBH specimen a_N = 0mm by the first order MVCCI method, (a) Δh = 4mm, (b) Δh = 2mm (curved l steps with marked mid-side nodes)

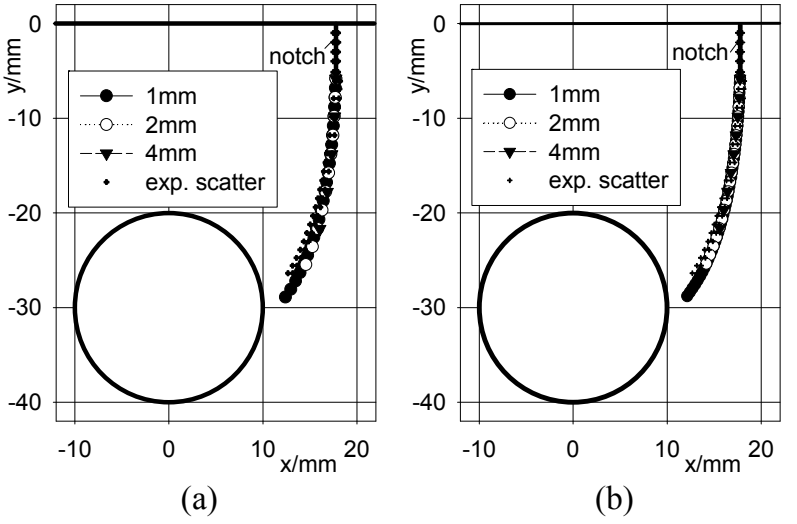

Figure 17: Simulated crack paths of LFBH specimen a_N = 18mm by the first order MVCCI method with different step width Δh and different methods, (a) MMI, (b) PCM (curved steps with marked mid-side nodes)

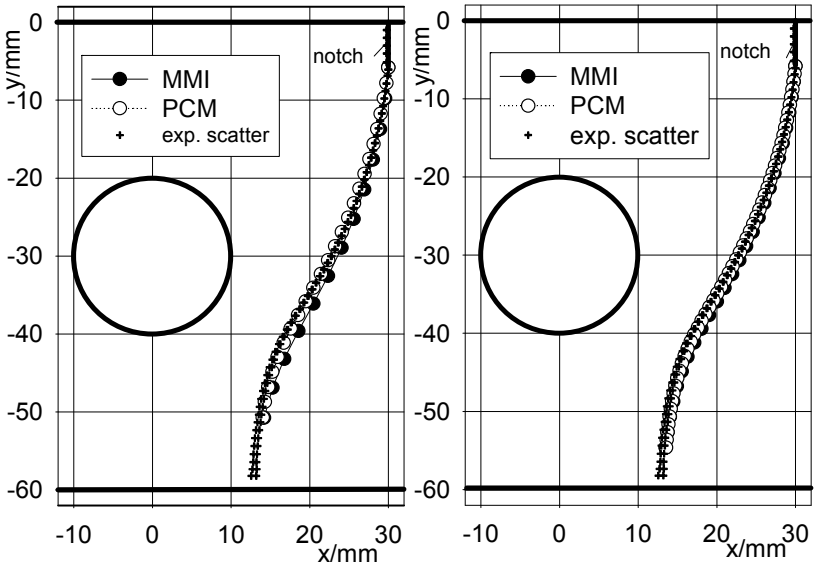

Figure 18: Simulated crack paths of LFBH specimen a_N = 30mm by the first order MVCCI method, (a) Δh = 4mm, (b) Δh = 2mm. (curved steps with marked mid-side nodes)

Table 3: Numerical results for the plastic limit load of a centrally cracked strip under tension

a/mm	σ_e/Nmm^{-2}		
	FKM	PCCS-2D	$\Delta\sigma_e$/%
2	203.67	206.35	+1.32
3	188.00	190.98	+1.59
4	172.33	175.17	+1.64
5	156.67	160.54	+2.47
6	141.00	144.24	+2.29
7	125.33	128.90	+2.85
8	109.67	113.15	+3.17
9	94.00	97.50	+3.72

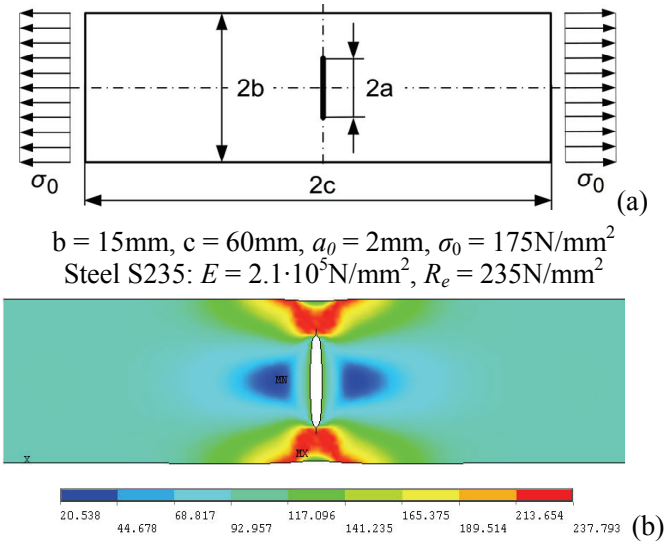

Figure 19: Centrally cracked strip under tension, (a) Geometry and material properties, (b) Equivalent stress distribution (v. Mises) σ_{eq}/Nmm^{-2} for the plastic limit load at a = 9mm

fastener holes has been studied, Fig. 23. In the given case the initial crack lengths are chosen as a_0 = 0.2mm. The sheet is subjected to tensile stresses σ_a at the lower edge and σ_b at the upper edge to realize the balance with the pressure at the holes. Two load cases are considered and the problems where simulated with a step width Δh_{lmax}= 0.4mm. In Fig. 23 the different computationally simulated crack trajectories for the five interacting cracks are shown. The non-dimensional stress intensity factor of the crack1 is given in Fig. 23c for the load case with $\sigma_b = \frac{1}{2}\sigma_a$. As crack lengths a_1 the arc lengths of the curved crack are chosen. The stress-intensity factor follows from

$$K_{I1} = \sigma_a \sqrt{\pi a_1} f_{I1}. \tag{39}$$

4.3 Crack growth under biaxial proportional cycling loading

The importance of studying the effects of biaxial loading on the fracture behaviour of structures and materials has been recognised for many years. Especially the testing of biaxial planar specimens gives the possibility to study the mechanism of crack propagation and the rules of crack path formation under concise conditions. Based on the numerical and experimental results of the sample problems it is

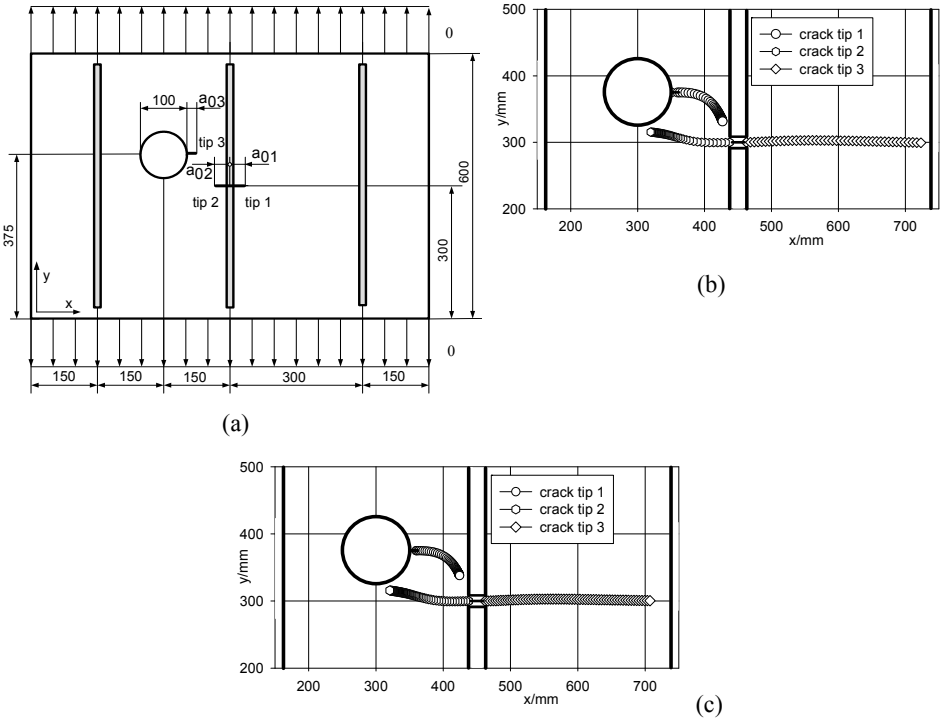

Figure 20: Multiple fatigue crack growth simulation in a stiffened panel (a), Δh_{lmax}= 6mm (b), Δh_{lmax}= 4mm (c) Material: A2024-T3, Young's Modulus:E = 78500MPa, Poisson's ratio: ν = 0.32, Paris law coefficients: C = 0.183*10^{-11}, n = 3.248

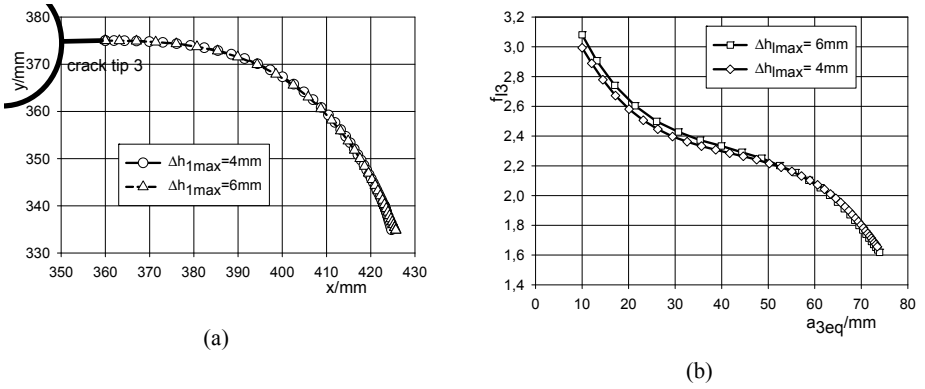

Figure 21: Simulated Crack paths of crack tip 3 of the stiffened panel (a) with the normalized stress intensity factor (b)

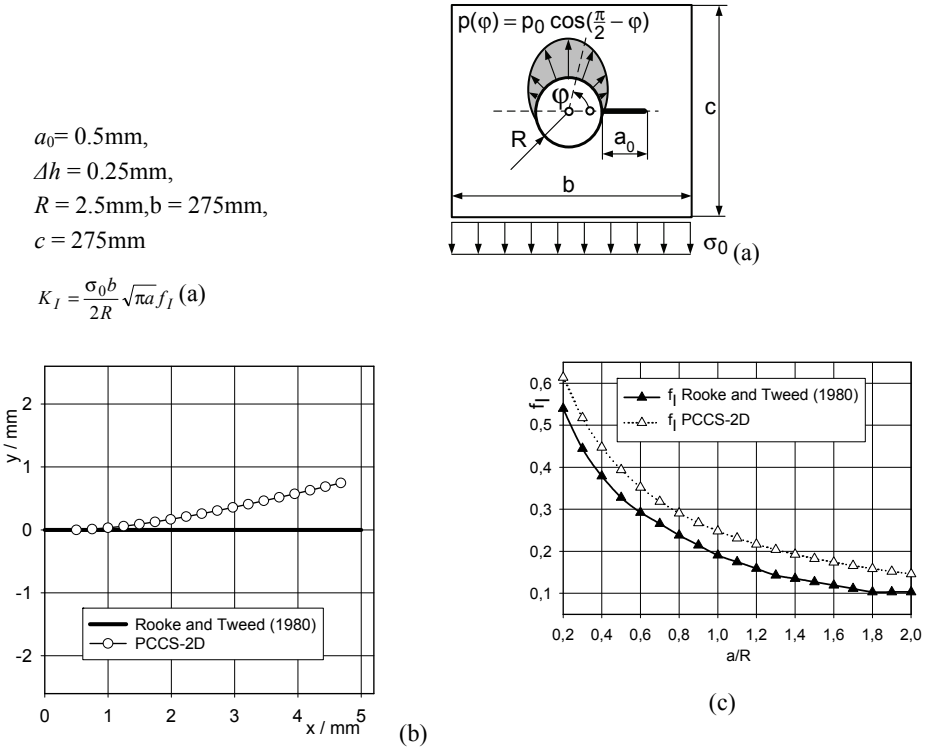

Figure 22: Crack path (b) and normalized stress intensity factor (c) of a crack at the edge of a pressurized hole

also possible to verify numerical simulation methods for more complex structures [Theilig, Hartmann, Wünsche, Henkel and Hübner (2007)].

The biaxial numerical and experimental investigations were done using cruciform slotted samples with a flat-bottomed square gage area, Fig. 24. This geometry effectively decouples the adjacent loading arms and means that the majority of the force on either axis is carried by the gage area over which the stress field is substantially uniform. In this case especially curved cracks emanating from a notch nearby the corner of the gage area with variation of angle ϕ are analysed for two different load ratios between the load axes. Fatigue crack growth was simulated until long curved cracks are formed, Fig. 25a. The initial notch lengths are chosen as a_0 = 1mm. The problems are analysed with a virtual crack extension increment Δh= 0.6mm.

The crack path tests were carried out with different stress ratios λ and two different

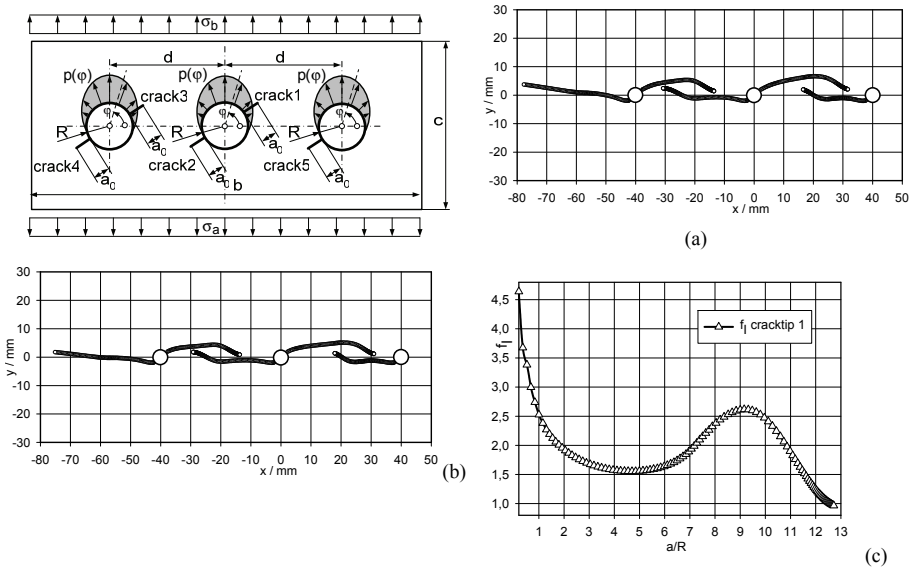

Figure 23: Crack paths of three inclined cracked pressurized holes for$\sigma_b = \frac{1}{2}\sigma_a$ (a) and $\sigma_b = \frac{3}{4}\sigma_a$ (b) with normalized stress intensity factor of the crack1 for $\sigma_b = \frac{1}{2}\sigma_a$ (c), a_0= 0.5mm, ϕ_0= 40°, R = 2.5mm, b = 150mm, c = 240mm, d = 40mm, Δh_{lmax}= 0.25mm, E = 65500MPa, ν = 0.34, n = 2

load ratios R. A stepwise decrease of the load was applied so that the crack growth rate stayed below 10^{-4} mm/cycle. All tests were done using sine wave proportional loading with a test frequency of 30 Hz. Fig. 25b shows the experimental results of two different R-ratios for the same crack configuration. It is seen that the higher (R = 0.3) value gives a better accordance to the prediction than R = 0.1. It seems to be that crack closure effects influence the crack path. In this case a proportional load case might no longer be supposed. Further experimental findings are shown in Fig. 25c with ϕ = 90°, λ= 0.5, R= 0.3.

4.4 Fracture Assessment by the FAD

In Fig. 26 an example of fracture mechanical assessment by the FAD procedure in combination with a numerical crack path simulation is given. The problem is a strip with shoulder and surface crack at the notched region under bending. The step width for the path simulation was Δh = 2mm. Failure by plastic collapse is expected under the given load and the used material at a crack length of about a_c = 8mm.

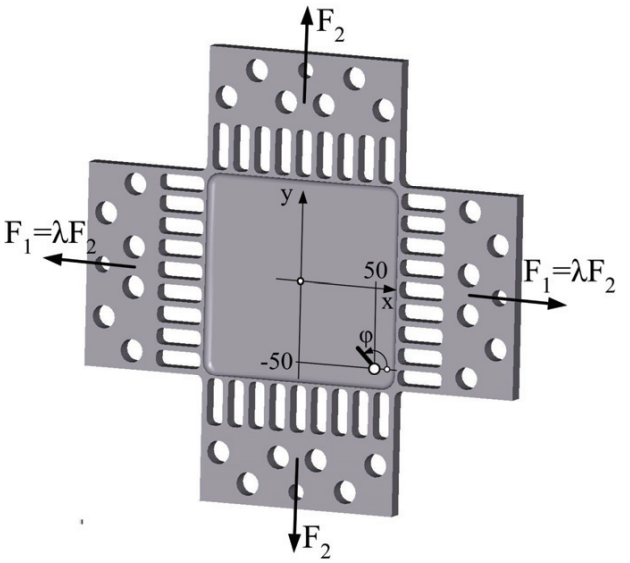

Figure 24: Geometry of the cruciform specimen with notches nearby the edge of the gage area

5 Summary and conclusions

The investigations presented and summarised in this paper have shown that the step-by-step higher order simulation process with a piece-by-piece parabolic curved approximation of the crack path offers a powerful method for the numerical analysis of crack growth in complex two-dimensional structures also for problems with multiple cracks.

The developed predictor-corrector procedure in combination with the improved MVCCI method provides excellent crack path simulation results with 8-noded quadrilaterals and only moderately refined finite element meshes around the crack tips.

From the extremely good correspondence of the numerical and experimental results one can conclude that the applied criterion of local symmetry provides a correct and reliable theoretical basis.

The proposed methods provide a robust concept to carry out flaw assessment with the FAD procedure in combination with a numerical crack path simulation.

Numerical examples are presented and discussed to demonstrate the efficiency and accuracy of the solutions.

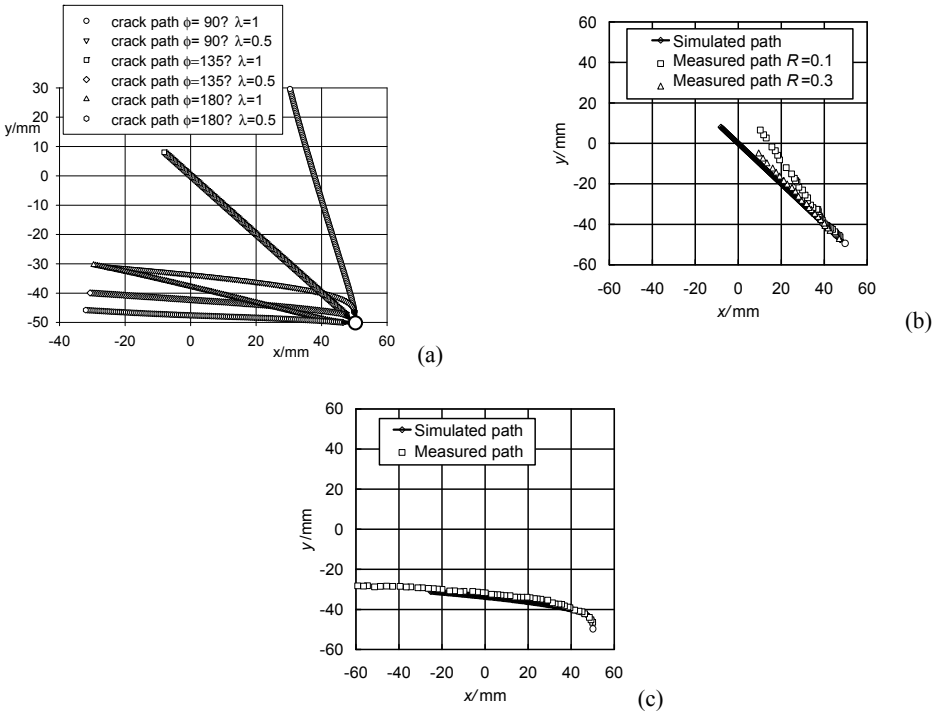

Figure 25: Simulated crack trajectories for the cruciform specimen with different initial crack directions ϕ and loading ratios λ (a), simulated crack path and influence of R-value on the crack growth paths for $\phi = 135^{\circ}$, $\lambda = 1$, (b), numerical and experimental crack path for a crack with $\phi = 90^{\circ}$, $\lambda = 0.5$, $R = 0.3$ (b)

Acknowledgement: In the scientific field of simulation of crack growth by the MVCCI method a laudable cooperation was over a period of more than 20 years with my colleague Prof. Dr. Gerhard-Friedrich Buchholz. He has always selflessly supported my scientific work. The author wishes to thank him posthumously for his critical discussions and contributions.

References

Aliabadi, M. H. (2002) *The Boundary Element Method Volume 2, Applications in Solids and Structures*, John Wiley & Sons.

Berger, Ch.; Blauel, G.; Hodulak, L.; Pyttel, B.; Varfolomeyev, I. (2006): *Bruchmechanischer Festigkeitsnachweis für Maschinenbauteile.* VDMA-Verlag, Frankfurt am Main.

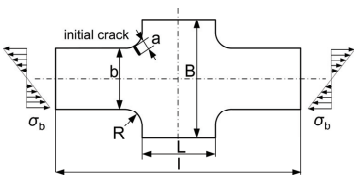

(a)

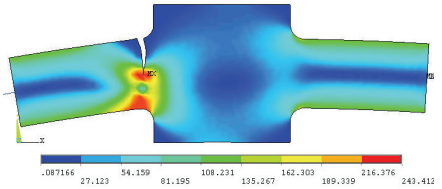

(b)

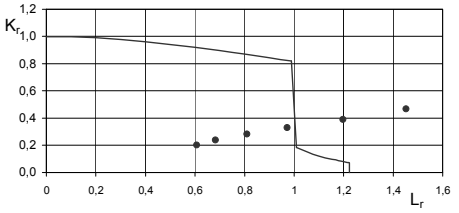

(c)

$B = 60\text{mm}$, $b = 30\text{mm}$,
$L = 60\text{mm}$, $l = 180\text{mm}$,
$R = 6\text{mm}$,
$a_0 = 2\text{mm}$, $\sigma_b = 175\text{N/mm}^2$
Steel S235:
$E = 2.1 \cdot 10^5\text{N/mm}^2$,
$R_e = 235\text{N/mm}^2$,
$K_{IC} = 3000\text{N/mm}^{3/2}$

a/mm	K_r	L_r
4	0.203	0.608
6	0.239	0.682
8	0.281	0.810
10	0.330	0.973
12	0.390	1.197
14	0.467	1.452

(d)

Figure 26: Simulation results for the strip with shoulder and surface crack at the notched region under bending, (a) geometry of the problem, (b) equivalent stress distribution (v. Mises) $\sigma_{eq}/\text{Nmm}^{-2}$ for the plastic limit load at $a = 14\text{mm}$, (c) failure assessment diagram with assessment points, (d) dimensions, material properties and results for the assessment points

Bergkvist, H.; Gnex, L. (1978): Curved crack propagation. *Int. J. of Fracture*, vol. 5, pp. 129-441.

Colombo, D.; Giglio, M. (2006): A methodology for automatic crack propagation modelling in planar and shell FE models. *Engineering Fracture Mechanics*, vol. 73, pp. 490-504.

Erdogan, G., Sih, G.C. (1963): On the crack extension in plates under plane loading and transverse shear. *J. Basic Eng.*, vol. 85, pp. 519-527.

Goldstein, R. V.; Salganik, R. L. (1974): Brittle fracture of solids with arbitrary cracks. *Int. Journ. of Fracture*, vol. 10, pp. 507-523.

Hull, D. (1993): Tilting cracks: the evolution of fracture surface topology in brittle solids. *Int. Journal of Fracture*, vol. 62, pp. 119-138.

Moës, N.; Dolbow, J.; Belytschko, T. (1999): A finite element method for crack growth without remeshing. *Int. J. Numer. Meth. Engng.*, vol. 46, pp. 131-150.

Rao, B. N., Rahman, S. (2000): An efficient meshless method for fracture analysis of cracks. *Computational Mechanics*, vol. 26, pp. 398-408.

Schöllman, M.; Fulland, M.; Richard, H. A. (2003): Development of a new software for adaptive crack growth simulations in 3D structures. *Engineering Fracture Mechanics*, vol. 70, pp. 249–268.

Sumi, Y. (1985): Computational crack path prediction. *Theor. Appl. Fract. Mech.*, vol. 4, pp. 149-156.

Sumi, Y.; Wang, Z. N. (1998): A finite-element simulation for a system of growing cracks in a heterogeneous material. *Mechanics of Material*, vol. 28, pp. 197-206.

Theilig, H. (1981): Verbesserte Berechnung von Spannungsintensitätsfaktoren mit finiten Elementen nach der Energiemethode. *Maschinenbautechnik*, vol. 30, pp.79-83.

Theilig, H. (1982): Dreidimensionale Analyse einer Kompaktzugprobe mit finiten Elementen. *Kernenergie*, vol.33, pp. 173-176.

Theilig, H. (1984): Erfahrungen bei der Anwendung der Energiemethode zur Berechnung von Spannungsintensitätsfaktoren mit der FEM. *Technische Mechanik*, vol.5, pp. 31-35.

Theilig, H.; Nickel, J. (1987): *Spannungsintensitätsfaktoren.* Fachbuchverlag Leipzig.

Theilig, H.; Döring, R.; Buchholz, F.-G. (1997): A higher order fatigue crack path simulation by the MVCCI-method. In: *Advances in Fracture Research*, ICF9, Volume 4, pp. 2235-2242, B. L. Karihaloo, Y.-W. Mai, M. I. Ripley, R. O. Ritchie, (Eds.). Pergamon, Amsterdam-Oxford-New York-Tokyo-Lausanne 1997.

Theilig, H.; Buchholz, F.-G. (2001): Curved Crack path prediction by the MVCCI-method and experimental verification for a specimen under lateral force bending.In: *Advances in Fracture Research*, ICF10, K. Ravi-chandar, B.L. Karihaloo, T. Kishi, R.o.Ritchie, A.T.Yokobori Jr, T.Yokobori, (Eds.) Published by Elsevier Science Ltd, Oxford, UK.

Theilig, H.; Wünsche, M.; Bergmann R. (2003): Numerical and experimental investigation of curved fatigue crack growth under proportional cyclic loading. *steel research*, vol.74, pp. 566-576.

Theilig, H.; Wünsche, M. (2005): Numerical simulation of fatigue crack propagation for 2D multiple crack problems by the MVCCI method. In: *Advances in*

Fracture and Damage Mechanics IV, M.H. Aliabadi, F.-G. Buchholz, J. Alfaite, J. Planas, A. Abersek, S.I. Nishida, (Eds.), EC, Ltd., UK.

Theilig, H.; Goth, M.; Wünsche, M. (2006): Numerical simulation of fatigue crack growth for curved cracks emanating from fastener holes in sheets by the MVCCI method. *Key Engineering Materials*, vols. 324-325, pp.857-860.

Theilig, H.; Hartmann, D.; Wünsche, M.; Henkel, S.; Hübner, P. (2007): Numerical and experimental Investigations of Curved Fatigue crack growth under biaxial proportional cyclic loading. *Key Engineering Materials*, vols. 348-349, pp.857-860.

Theilig, H.; Holländer, D.; Wünsche, M. (2010): Simulation of curved fatigue crack growth with calculation of the plastic limit load. *Key Engineering Materials*, vols. 417-418, pp. 45-48.

Tong, P.; Pian, T. H. H. (1973): On the convergence of the finite element method for problems with singularity. *Int. J. Solids Structures*, vol. 9, pp. 313-321.